Title
Modeling Hyperpolarized 13C Pyruvate And Urea Concentration Kinetics With Multiband RF Excitation MRI In Prostate Cancer

Author
Bahrami, Naeim

Publication Date
2013

Peer reviewed|Thesis/dissertation

Modeling Hyperpolarized ^{13}C Pyruvate And Urea Concentration Kinetics With Multiband RF Excitation MRI In Prostate Cancer

by

Naeim Bahrami

THESIS

Submitted in partial satisfaction of the requirements for the degree

of

MASTER OF SCIENCE in Biomedical Imaging

in the

GRADUATE DIVISION

of the

UNIVERSITY OF CALIFORNIA, SAN FRANCISCO

[redacted]

Acknowledgement

I want to thank my supporting parents, my lovely brother and my two wonderful sisters for their incredible support in everything I do and for inspiring me to do my best. I appreciate them for their boundless commitment to developing my education and for cultivating and fostering in me the values necessary to succeed. I would also like to acknowledge all of the individuals that have provided the training, knowledge, and assistance in the completion of this work. Specifically, Dr. Peder Larson for allowing me to work in her lab while consistently teaching me and guiding me through the thesis process. In addition, I would like to thank members of the Subeck lab: Cornelius Van Morze for helping with understanding some concepts and programing protocol, Galen, Peter Shin, and Christine for being my go-to mentor in all things technical. I would also like to thank other members of my thesis committee: Dr. David Saloner, Dr. John Kurhanexicz, and Dr. Susan Noworolski for their thorough evaluation of my thesis. Finally, I would like to thank the MSBI program and the UCSF department of Radiology for all resources that have been provided throughout the year that terminated in the completion of this thesis.

Modeling Hyperpolarized ^{13}C Pyruvate And Urea Concentration Kinetics With Multiband RF Excitation MRI In Prostate Cancer

by

Naeim Bahrami

Abstract

The accurate detection and characterization of cancerous tissue is still a major problem for the clinical management of individual prostate cancer patients and for monitoring their response to therapy. ρ_1 (TR times to times points per second over T1 ratio) of urea, pyruvate, lactate, and alanine, also the amount urea and pyruvate perfusion, and conversion constant between pyruvate to lactate(Kpl) and pyruvate to alanine(Kpa) are important parameters in different organs including cancerous and healthy tissues. ρ_1 of urea in kidneys, prostate cancerous tissues, and liver are measured 0.13(1/s), 0.15(1/s), and 0.075(1/s), respectively and ρ_1 of pyruvate in kidneys, liver cancer and healthy part of liver is 0.08(1/s), 0.13(1/s), and 0.064(1/s), respectively with TR=250ms. Kpl in cancerous tissues are more than 0.44(1/s) which is significantly higher than Kpl of metabolites in healthy tissues (Kpl = 0.028(1/s)) with p value less than 0.001. This Kpl is proportional to the lactate signal to pyruvate signal ratio with Correlation Coefficient=0.95. High perfusion amount of the accumulation of pyruvate, lactate, and alanine in compare to urea perfusion has been seen in cancerous tissues (liver cancer and prostate cancer) significantly ($p<0.001$) less than in healthy tissues.

Table of Contents

LIST OF FIGURES

LIST OF TABLES

Introduction

The accurate detection and characterization of prostate cancer is still a major problem for the clinical management of individual prostate cancer patients and for monitoring their response to therapy. Recent technological advances in ^{1}H Magnetic Resonance Spectroscopic Imaging (MRSI) have made it possible to correlate in-vivo prostatic citrate concentrations with the presence of prostate cancer. According to the analysis of human prostate tissue samples and results obtained from animal models of prostate cancer, it has been hypothesized that the observed decrease in citrate with prostate cancer is associated with increased citrate oxidation in the citric acid cycle, increased fatty acid synthesis, and/or increased glycolytic lactate production[1]. MRSI with hyperpolarized ^{13}C labeled substrates is a new method to study prostate cancer that may be able to simultaneously and noninvasively evaluate changes in metabolic intermediates from multiple biochemical pathways of interest and thereby explain the observed changes in prostatic citrate concentrations.

Recent studies have shown a large amount of potential applications of hyperpolarized (HP) ^{13}C MRSI for the in vivo monitoring of cellular metabolism and the characterization of disease [2, 3]. The low natural abundance and sensitivity of ^{13}C compared to the protons poses a technical challenge using conventional approaches[4]. Dynamic nuclear polarization (DNP) of ^{13}C labeled pyruvate and subsequent rapid dissolution generates a contrast agent with a four order-of-magnitude sensitivity enhancement that is injected and gives this ability to monitor the spatial distribution of pyruvate and its conversion to lactate, alanine, and bicarbonate [5]. The conversion of pyruvate to lactate catalyzed by the enzyme lactate dehydrogenase is of particular interest, as the kinetics of this process have been shown to be sensitive to the presence and severity of disease in preclinical models [6].

The assessment of early response to targeted therapies using conventional imaging methods such as magnetic resonance imaging (MRI) or computerized tomography (CT) remains a challenge. MRI and CT are mostly limited to the detection of anatomical changes, which typically occur at late time points post treatment initiation. These changes can be as drastic as tumor shrinkage, but treatment can also induce tumor stasis or inhibition of tumor growth. In such cases, anatomical imaging methods are unable to provide an early indication of tumor responsiveness to molecularly targeted treatments[7, 8].

The transgenic adenocarcinoma of mouse prostate (TRAMP) murine model is a well-characterized model of prostate cancer that mimics the rapid disease progression, histopathology and metabolic changes observed in human disease[9, 10]. These mice are widely used in the identification of novel biomarkers and molecular mechanisms associated with disease progression, as well as in the investigation of new strategies for characterizing and treating human prostate cancers. The use of histopathology as the definitive end point in evaluating disease progression and treatment efficacy is subjective, with significant differences between individual pathologists interpretation, and prevents the serial assessment of the associated cellular bioenergetic pathways over time. Mice prostate cancer studies would therefore greatly benefit from in vivo metabolic imaging using ^{13}C MRSI. We used these mice as a model system of human prostate cancer to test the proposed fitting methods.

The value of T1 reflects the dynamics of nuclear spin. For low-sensitivity nuclei the estimation of ρ_1 (the ratio of TR to T1) with hyperpolarized samples is not made by the classical inversion-recovery method because repeated hyperpolarizations would be too time consuming and expensive[11]. Instead the measurement of T1 and ρ_1 is done with the sample hyperpolarized by subjecting it to multiple small angle pulses in quick (relative to T1 and ρ_1) succession. Thus we acquire a series of longitudinal magnetization measurements from each RF pulse. The problem with this approach for

pyruvate in vivo is that each RF pulse subtracts some of the magnetization(Pyruvate) from the sample in addition to conversion to Lactate. Repeated sampling of small amounts of the magnetization at regular time intervals yields an exponentially decaying signal (even if longitudinal relaxation were not operating) in such a way that the relaxation time that characterizes the exponential decay is in general smaller than that of the intrinsic T1.

The variation of the signal that is detected in perfusion imaging of each tissue including cancer reflects spatially heterogeneous changes to existing vasculature and neovascularization as tumors surpass the normal blood supply, including microcirculatory disturbance in some of the abnormal vessels[12]. Besides tumor perfusion data the metabolic data available from spectroscopic imaging of [1-13C]pyruvate [13] would also be of important value in exploring the complex relationship between perfusion and metabolism in cancer at both preclinical and clinical research levels[14].

An important consideration for performing hyperpolarized 13C MR studies is the T1 relaxation time of the unrecoverable spin polarization after dissolution of the polarized sample. Specifically, if metabolically active substrates such as [1-13C] pyruvate are used to probe real time metabolism in vivo or in vitro, reduced T1 may limit the spatial resolution and temporal lifetime of the study[15]. In this study, the field dependence of solution state T1 relaxation times of hyperpolarized [1-13C] pyruvate is exploited by using a relatively low magnetic field, 3T (31MHz), to retain higher amounts of residual polarization.

The primary purpose of this research was to model dynamic changes in HP pyruvate and urea to provide improved characterization of cancerous tissues when using arbitrary RF flip angles in dynamic MRSI. Data was acquired on mice with prostate cancer and comparisons were made to normal tissues such as kidney or liver of the metabolite concentrations, including Urea, Pyruvate, and Lactate, the conversion constant (Kpl) between pyruvate to lactate, and the conversion constant

(Kpa) between pyruvate to alanine. We used two different fitting approaches to achieve this aim: an approach which is enabled by calculating the longitudinal magnetization and differential of longitudinal magnetization and extracting parameters including ρ_1 values of the metabolites, Kpa, and Kpl. The other fitting approach was based on a non-linear least square algorithm to fitting the parameters in the kinetic model (metabolite T1values, Kpa, and Kpl). We also created novel parameterizations of the total pyruvate and urea perfusions in order to assess vascular delivery and tissue uptake. A key new feature of these methods is their ability to detect metabolic conversion, magnetization exchange between compounds, and perfusion when using arbitrary RF flip angles on the different compounds.

Methods and Materials

Data acquisition

The 13C MRSI data was acquired with 18-fold acceleration using a compressed sensing pulse sequence[16]. The repetition time (TR) was 250 ms and images were reconstructed every 2 sec. Imaging started at the end of a 12 sec injection of 350 µL of 80 mM [1-13C]pyruvate and 80 mM 13C-urea. The images had 5x5x5.4 mm spatial resolution and a matrix size of 12x12x16 for full mouse coverage. The sequence implemented uses multiband spectral spatial RF pulses [17] while allowing for different excitation angles imparted to pyruvate, lactate, alanine and urea. Small flip angles of 6 degrees for urea and pyruvate were used to minimally perturb their magnetization while larger flip angles of 12 degrees for lactate and alanine were used to increase the SNR. This small flip angle on pyruvate is expected to yield a greater cumulative signal on lactate since depolarization is reduced[18]. All imaging was acquired from a GE Healthcare 3T MRI at Byers Hall. Subjects used

for this study were 4 TRAMP mice with prostate cancer and 3 double transgenic mice with liver cancer[19].

Pyruvate and Urea Kinetics

The kinetics of the HP pyruvate magnetization can be modeled as:

$$\frac{d}{dt}\begin{bmatrix} Mp(t) \\ Ml(t) \\ Ma(t) \end{bmatrix} = \begin{bmatrix} -\rho_p - Kpl - Kpa & 0 & 0 \\ Kpl & \rho_l & 0 \\ Kpa & 0 & \rho_a \end{bmatrix} \begin{bmatrix} Mp(t) \\ Ml(t) \\ Ma(t) \end{bmatrix} \quad (1)$$

where ρ_p, ρ_l, and ρ_a, are the longitudinal magnetization relaxation rates for pyruvate, lactate and alanine, respectively, Kpl is the conversion rate from pyruvate to lactate, and Kpa is the conversion rate from pyruvate to alanine. We assume the reverse conversion rates are negligible.

Equations 2 through 5 show the solution to the kinetic model as well as for urea of the longitudinal magnetization:

$$Mzu(t) = Cu.e^{-(\rho_u)t} \quad (2)$$

$$Mzp(t) = Cp.e^{-(Kpl+Kpa+\rho_p)t} \quad (3)$$

$$Mzl(t) = \frac{Cp.Kpl}{\rho_l - Kpl - Kpa - \rho_p}.e^{-(Kpl+Kpa+\rho_p)t} + Cl.e^{-\rho_l t} \quad (4)$$

$$Mza(t) = \frac{Cp.Kpa}{\rho_a - Kpl - Kpa - \rho_p}.e^{-(Kpl+Kpa+\rho_p)t} + Ca.e^{-\rho_a t} \quad (5)$$

As it can be observed the lactate and alanine magnetization will decay based on the relaxation while there is some addition because of metabolite conversion from pyruvate.

Flip angle effects on the magnetizations and decaying of the signal occur after each RF pulse. The flip angle effects on the longitudinal magnetization between images can be described in the following equation:

$$\Delta M_{zx}[n] = \frac{S_x[n] - (M_{zx}[n-1].\sum_{k=1}^{N} sin\theta_x \,.\, (\cos\theta_x)^{k-1})}{\sin\theta_x} \quad (6)$$

Where x represents pyruvate, lactate, alanine, or urea, θ_x is the appropriate flip angle for the metabolites (12 degrees for lactate and alanine and 6 degrees for pyruvate and urea), N is the number of flip angles per image (N=8 in our data), and the signal S_x.

Linear Square and Non-Linear Square Method

There are several numerical methods for solving the non-linear kinetics of HP pyruvate and urea in the presence of metabolite specific flip angles. The value of ρ_1 for urea can be estimated from data acquired using an RF pulse sequence with fixed time-intervals between sampling flip pulses by fitting (nonlinear regression) a decaying exponential function to them. However, the pyruvate kinetics require a more complex approach.

First Approach – Linearized kinetics

First, we considered the magnitude of the longitudinal magnetization for extracting the parameters including ρ_1 values Kla, and kpl is shown in equation 1 while we are assuming that the conversion constant values from Lactate and Alanine(Klp and Kap, respectively) are zero. We created a linear system of equations by discretizing Equation 6 as $\frac{d}{dt}M_{zx} \approx \frac{1}{\Delta t}\Delta M_{zx}[n]$ combined with the flip angle effects in Equation 6. This was solved using weighted least-squares (WLS) where the weighting was the lactate signal, $S_{xL}[n]$.

Second Approach - Non-linear least squares

This approach is to use non-linear least squares (NLLS) to fit the signal based on Equations 6 and 5. For NLLS, the Levenberg–Marquardt's (LM) approach has been the method of choice, perhaps, due due to its simple implementation. This simplicity is due in part to its approximation to the Hessian matrix of the NLLS objective function. Another approach is Newton's method (or full Newton-type type method) where the complete Hessian matrix is required in the estimation process. It is well

known that Newton's method is more robust than the LM method and can speed up convergence in NLLS problems [20-23], but the complete Hessian matrix is often not available or known for a given problem.

This strategy entails using the WLS solution as the initial guess, adjusting the LM parameter, and incorporating the full Hessian matrix of the NLLS objective function. With estimation of ρ_1 values for metabolites like urea, pyruvate, lactate, and Kpl from the First Approach we will have a good initial condition. Entering the initial T1 and subsequently ρ_1 values and Kpl to create a new signal and extracting estimated and predicted ρ_1 values and Kpl from a non- linear least square method to solve the problem directly is a great procedure to have a better and more robust values. We also found that obtaining a good fit with our SNR required assuming that the relaxation rates, ρ_1, of pyruvate, lactate, and alanine were identical.

Perfusion Parameterization

Our studies included HP 13C-urea as an independent marker of perfusion. To quantify, this perfusion, we propose perfusion parameters of urea perfusion as well as total pyruvate perfusion, which accounts for conversion to lactate and alanine. For total pyruvate perfusion, we propose:

$$P_p = \int_0^\infty \widehat{M}_{zP}(t) + \widehat{M}_{zL}(t) + \widehat{M}_{zA}(t)\, dt \qquad (7)$$

Where P_p is pyruvate perfusion accumulation and $\widehat{M}$ is the longitudinal magnetization of pyruvate, lactate, and alanine as calculated by the kinetic model (ie without the influence of RF pulses). For the urea perfusion we propose:

$$P_u = \int_0^\infty \widehat{M}_{zU}(t)dt \qquad (8)$$

Where P_u is the urea perfusion and $\widehat{M}$ is the longitudinal magnetization of urea as calculated by the model. For an initial magnetization $M_{zU}[0]$ we have:

$$P_u = \int_0^\infty M_{zU}[0].\, e^{-t\,\rho_u} dt = M_{zU}[0]/\,\rho_u \qquad (9)$$

When we are assuming that ρ_l, ρ_a, and ρ_p are equal as in the non-linear least squares fitting, we can derive the accumulation of pyruvate perfusion as:

$$P_p = \int_0^{\infty} (M_{zP}[0] + M_{zL}[0] + M_{zA}[0]).e^{-t\,\rho_p} dt = (M_{zP}[0] + M_{zL}[0] + M_{zA}[0])/\,\rho_p \qquad (10)$$

(If ρ_l, ρ_a, and ρ_p are not equal, the full expressions from Equations 3-5 can be used.)

We also speculated that the ratio of total lactate signal to total pyruvate signal would be commensurate with Kpl. In other words, with summing all time points and assuming a constant ratio, we speculate:

$$\frac{\sum_{i=1}^{Nt} Li}{\sum_{i=1}^{Nt} Pi} = C * Kpl \qquad (12)$$

Where Nt is number of time points, Li and Pi are lactate and pyruvate peak values, respectively. This relationship is strictly true across different voxels provided we assume a constant lactate relaxation rate and delivery of pyruvate.

Results

Signal Estimation

HP ^{13}C MRSI and anatomical imaging were performed on seven mice. Fig.1 presents anatomical MR datasets from the prostate and kidney for one of the animals with prostate cancer and Fig. 2 shows the healthy tissue of kidney and liver for one the animals with liver cancer. HP ^{13}C pyruvate is detectable in each voxel of the grid, and is comparable between cancerous tissue and normal one. However, HP ^{13}C lactate signal is much higher in the tumor region. As we could expect the amount of pyruvate to lactate is much higher in cancerous tissue compared to normal tissues.

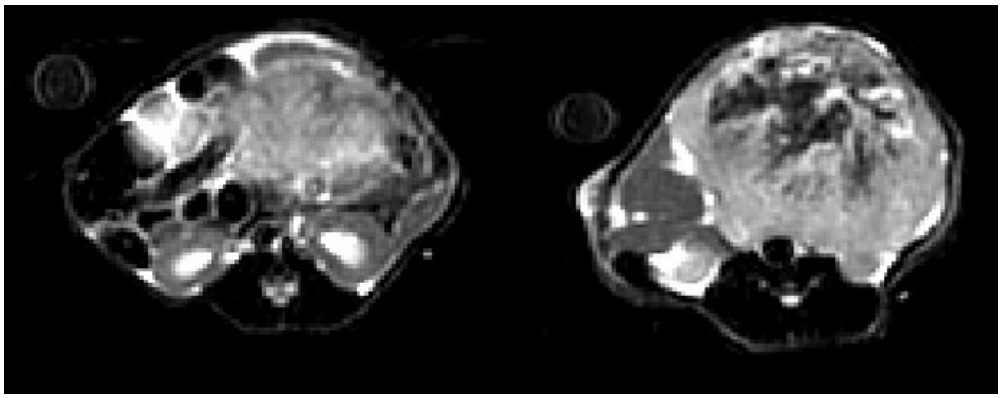

Figure 1. The image in the left shows a slice which is including the kidneys and the right one shows the prostate cancerous tissue in a TRAMP mouse.

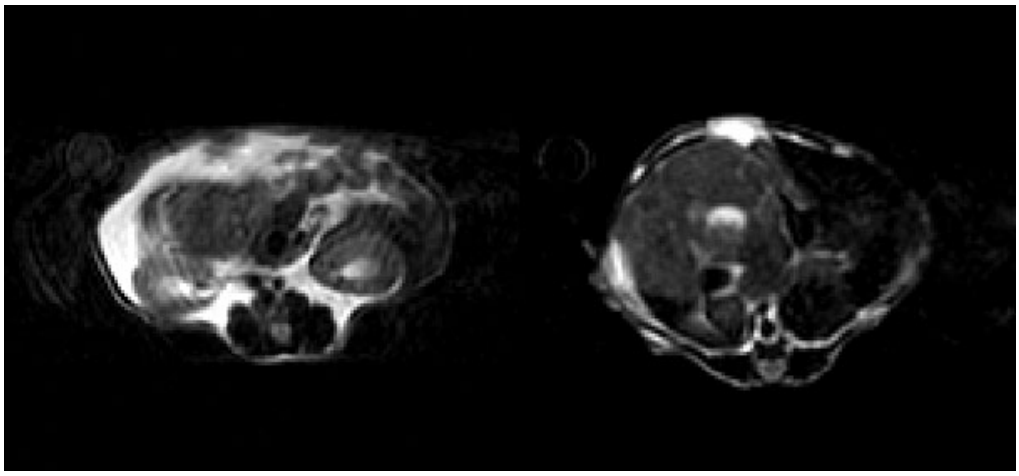

Figure 2. The image in the left shows a slice which is including the kidneys and the right one shows the cancerous liver tissue in a mouse with liver cancer.

The signal extracted from prostate and liver cancer voxels and the signal that was fit from the method using the difference longitudinal magnetization of the metabolites which was mentioned in the previous section are shown on Fig. 3 and Fig. 4, respectively.

In Fig. 3 and Fig. 4 the real signal of three metabolites including Pyruvate, Lactate, and Urea is presented and we can observe the noisy, approximately exponential decay. Estimation of final values

for the parameters can be generated from the longitudinal magnetization and difference of longitudinal magnetization in each image.

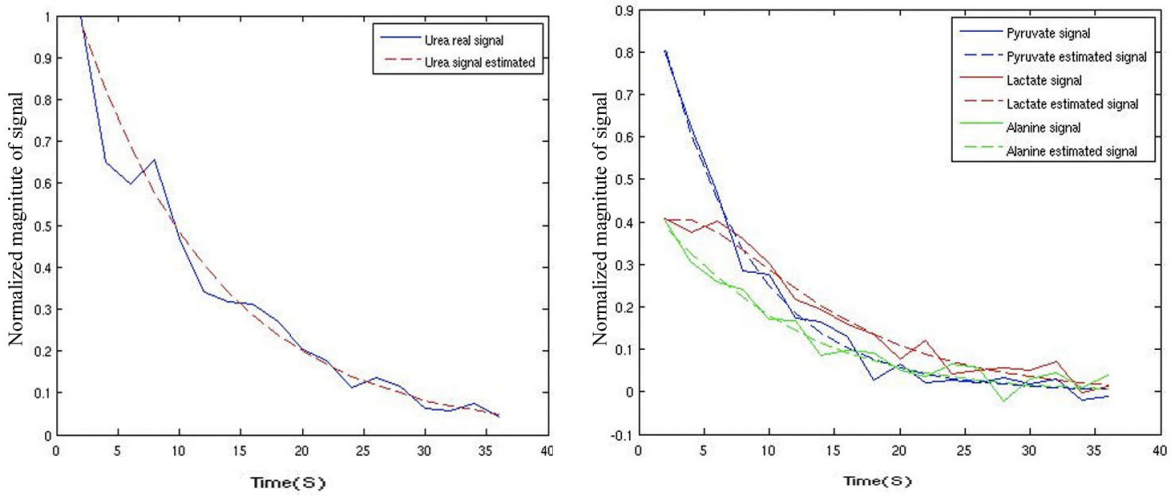

Figure 3. Real (solid) and fit (dashed) signal curves in a prostate tumor voxel using the method of longitudinal magnetization difference fitting for urea(left image) and pyruvate, lactate, and alanine(right image).

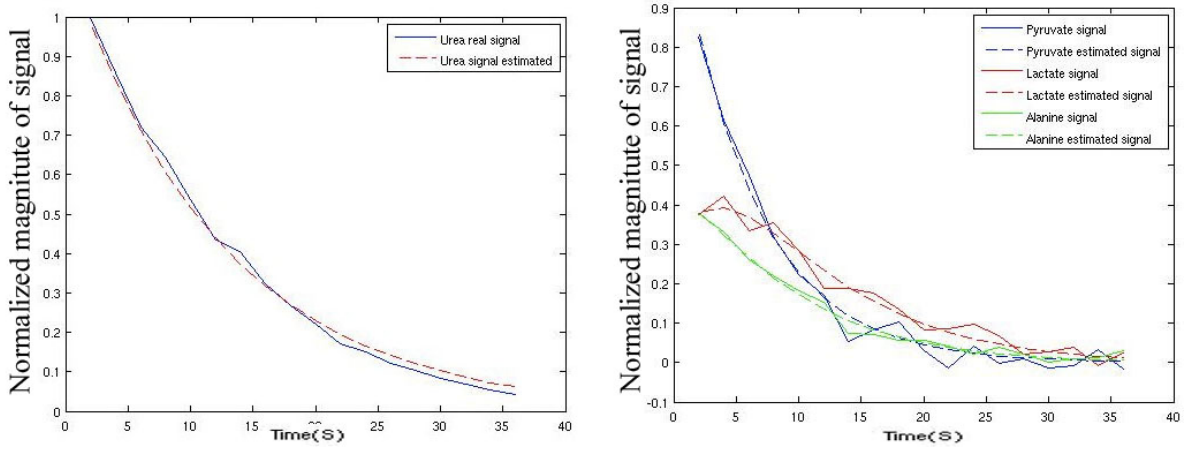

Figure 4. Real (solid) and fit (dashed) signal curves in a liver tumor voxel using the method of longitudinal magnetization difference fitting for urea(left image) and pyruvate, lactate, and alanine(right image).

Metabolites Characterizations

Table 1 and table 2 present the average metabolites' ρ_1 values, Kpl, and Kpa in the prostate and liver tumor tissues, respectively, based on the non-linear least square fitting method. According to previous studies[24-26] the in-vivo T1 values of HP ^{13}C urea and pyruvate are in range of 30s and 40s,respectively. Likewise, T1 values of lactate and alanine are in the same range as pyruvate [26, 27].

Table 1 Average ρ_1 values and conversion constant rates in prostate tumor, kidney, and liver for the animals with prostate cancer.

	ρ_1 of Urea (1/s)	ρ_1 of Pyruvate and its products(1/s)	Kpl(1/s)	Kpa(1/s)
Kidney	0.13	0.09	0.028	0.005
Prostate Tumor	0.15	0.083	0.044	0.011
Liver	0.075	0.061	0.032	0.006

Table 2 Average ρ_1 values and conversion constant rates in cancerous liver, healthy liver, and kidney for the animals with liver cancer.

	ρ_1 of Urea(1/s)	ρ_1 of Pyruvate and its products(1/s)	Kpl(1/s)	Kpa(1/s)
Kidney	0.08	0.084	0.022	0.003
Cancerous Liver	0.13	0.077	0.050	0.077
Healthy Liver	0.064	0.071	0.026	0.0033

In these studies, the ρ_1 measurements are larger than previous studies. This is likely due to acquisition imperfections (flip angle calibrations, loss during refocusing pulses) and flow loss of signal during the experiment [28]. In Fig. 5 the mean variation of ρ_1 value of pyruvate and its products has been presented in different tissues of prostate tumor mice. Significant differences ($p<0.001$) were found between tumor and liver, and also between kidney and liver showing that T1 values of the Pyruvate and its products and its metabolic products are higher in healthy tissues in liver with respect to cancerous prostate tissue.

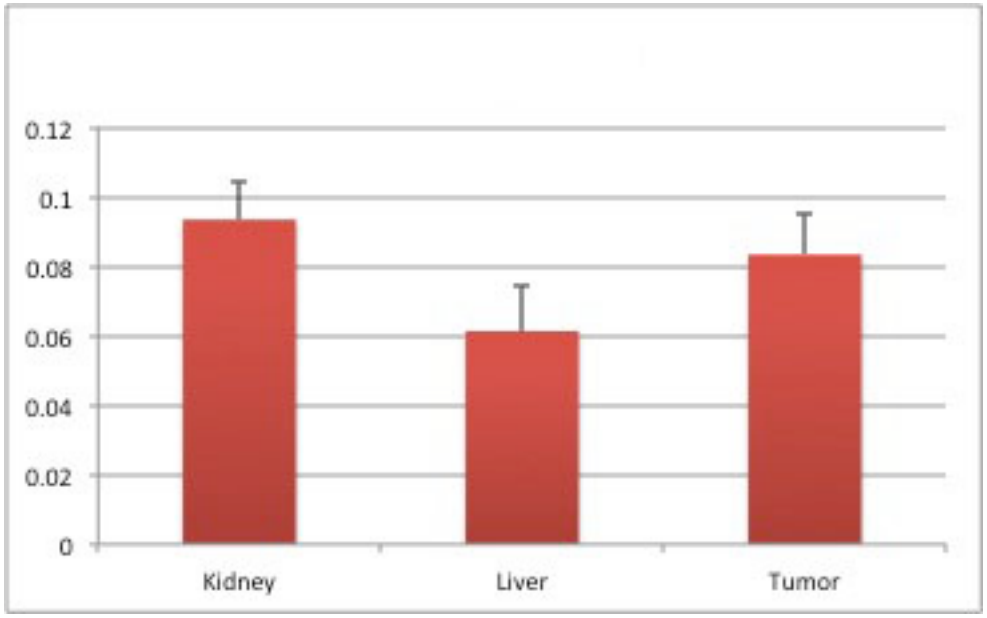

Figure 5. Pyruvate and its products ρ_1 (mean and standard deviation) in three different tissues among four animals that had prostate cancer.

Fig. 6 illustrates values and the variation of ρ_1 of the pyruvate and its products in different tissues of liver cancer mice. We calculated no significant differences between regions which suggests the T1 values of the Pyruvate and its products and its metabolic products are the same in healthy tissues in liver with respect to cancerous tissue.

In Fig. 7 the amount of ρ_1 of the urea has been presented in different tissues of prostate cancer mice. Significant differences were observed ($p<0.001$) between tumor and liver, and also between kidney

and liver showing that T1 values of the urea are higher in healthy tissues in liver and kidney with respect to cancerous prostate tissue.

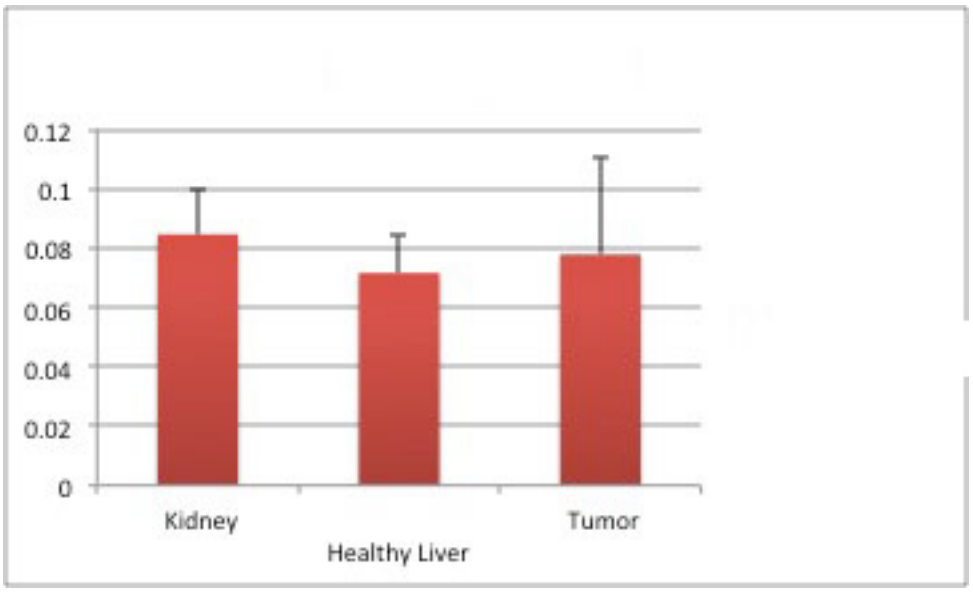

Figure 6. Pyruvate and its products ρ_1 in three different tissues among three animals that had liver cancer.

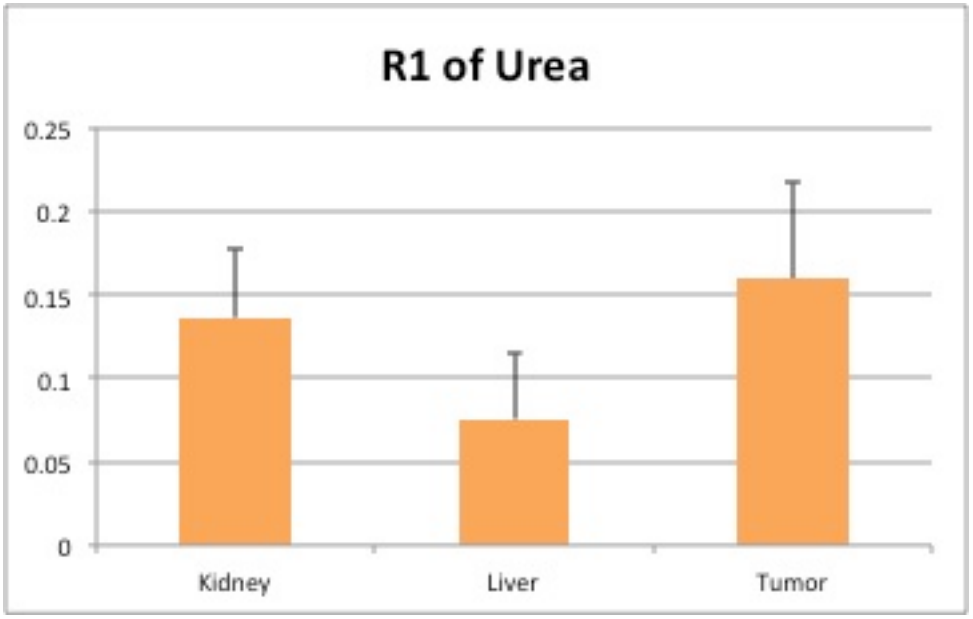

Figure 7. Urea ρ_1 in three different tissues among four animals that had prostate cancer.

Fig. 8 illustrates of ρ_1 value of the urea in different tissues of liver cancer mice. Significant differences were found (p=0.007) between healthy tissue and cancerous tissue in liver showing that ρ_1 values of the urea are lower in healthy voxels with respect to cancerous tissue.

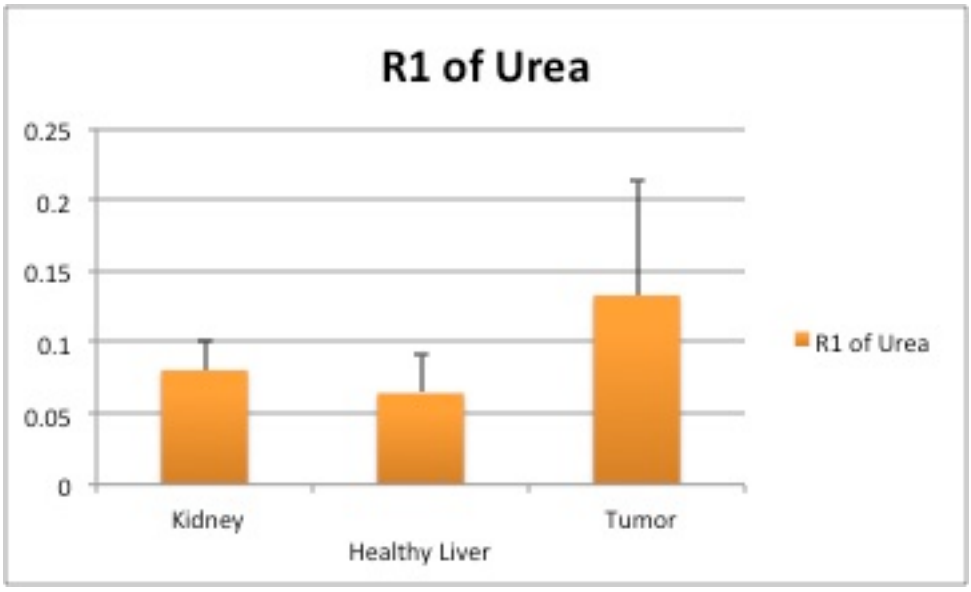

Figure 8. Urea ρ_1 in three different tissues among three animals that had liver cancer.

The conversion rate constant between metabolites (Kpl and Kpa) are markers of the tissue metabolic profile. Similarly to previous studies, higher Kpl was associated with cancerous tissue. In addition, Kpa variation was pretty low with respect to Kpl among all voxels. In Fig. 9 and Fig. 10 are shown the varying pattern of Kpl between the voxels of interests across all of the subjects. A significant difference was observed ($p<0.001$) between cancerous tissues and non-cancerous tissues.

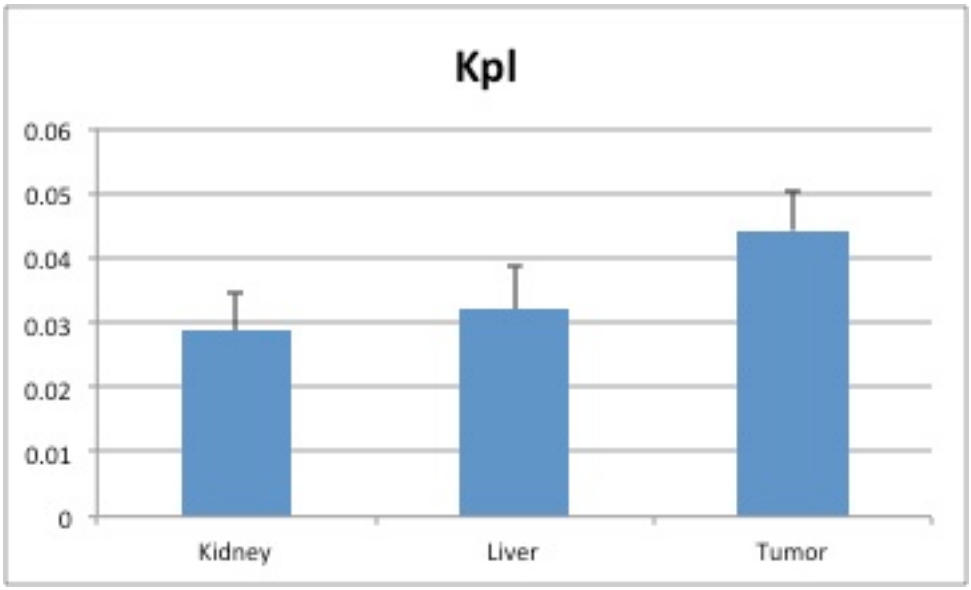

Figure 9. Kpl values in three different tissues among four animals that had prostate cancer.

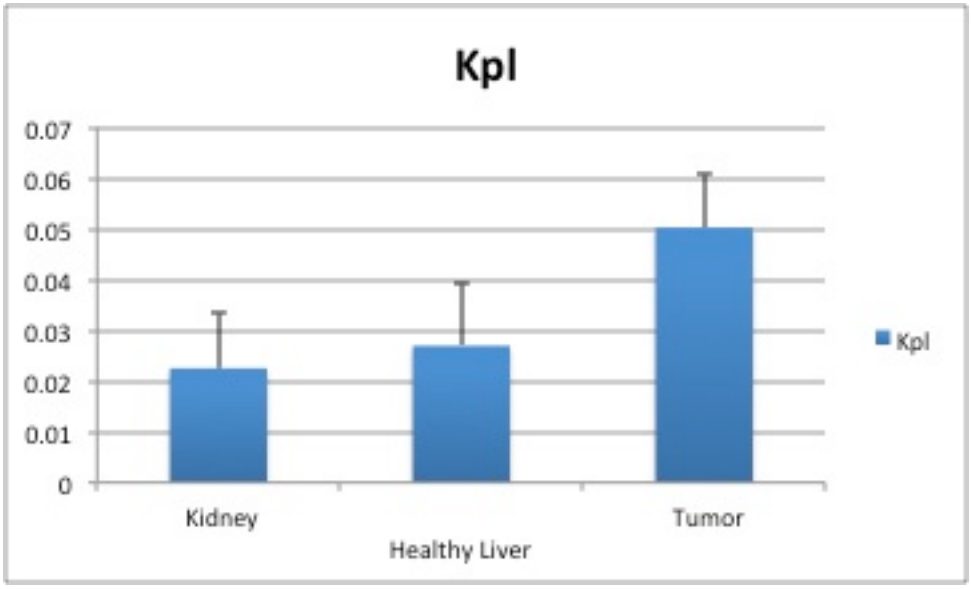

Figure 10. Kpl values in three different tissues among three animals that had liver cancer.

Perfusion Characterizations

We observed urea perfusion was relatively low in both prostate cancer and liver cancer tissue as presented in Fig. 11 and Fig.12.

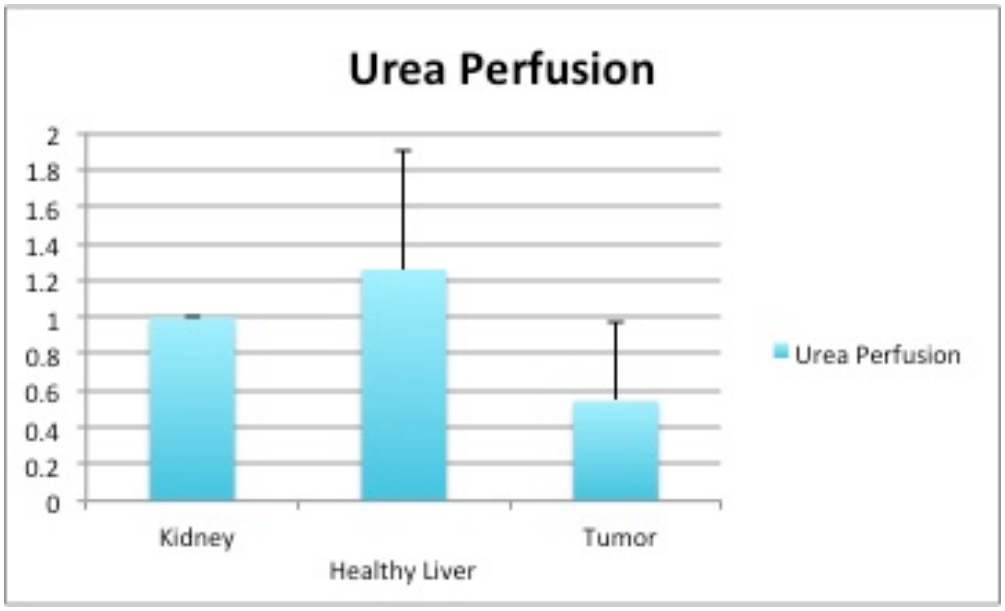

Figure 11. Urea perfusion extracted from four animals with prostate cancer. There was relatively low urea perfusion in the tumor tissue, and a significant difference ($p < 0.04$) between liver and tumor. (All metabolites' perfusion are normalized with the perfusion values in Kidney)

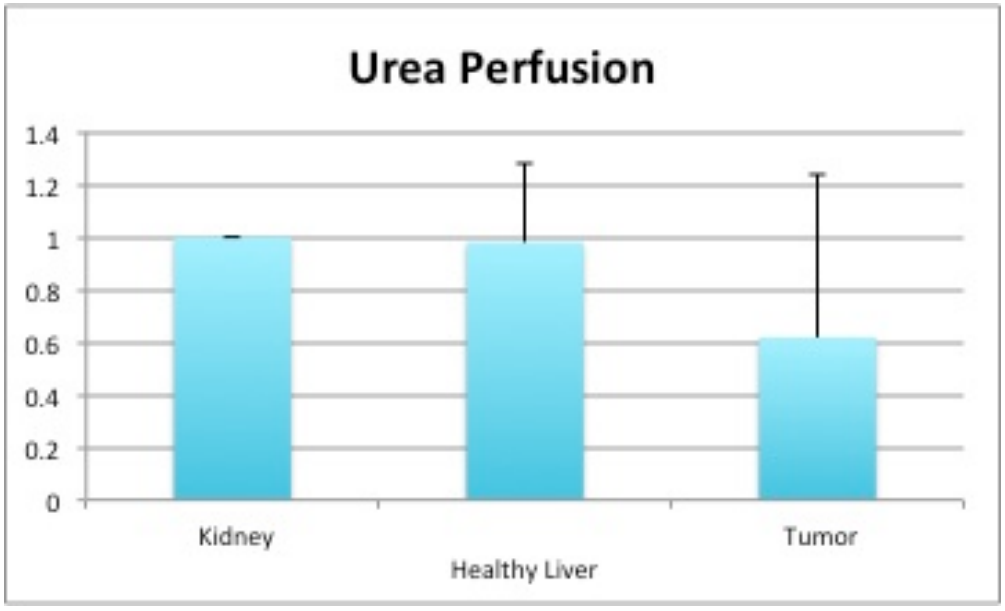

Figure 12. Urea perfusion extracted from three animals with liver cancer. There was relatively low urea perfusion in the tumor tissue, and a significant difference ($p < 0.03$) between kidney and tumor. (All metabolites' perfusion are normalized with the perfusion values in Kidney)

We normalized the perfusion rates to the kidney values. For this purpose the measured perfusion for each tissue such as healthy part of liver, tumor region of liver, prostate tumor, and kidneys are

divided by the measured perfusion of kidney, and this process is irritated for all metabolites including pyruvate and its products and urea. In Fig. 13. the ratio of Pyruvate and its products and its metabolic products perfusion over urea perfusion is shown.

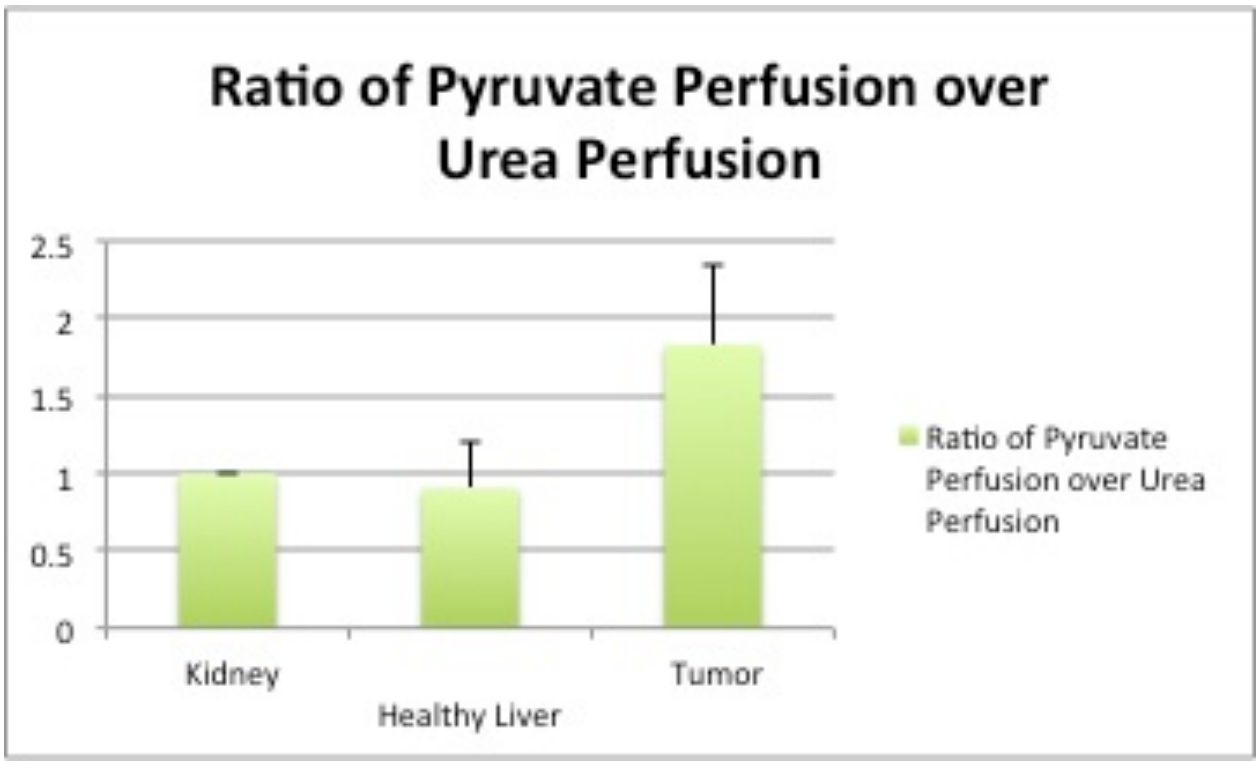

Figure 13. The perfusion ratio between metabolites. The ratio between tumor-kidney and tumor-healthy liver is significantly different ($p < 0.001$). (All metabolites' perfusion are normalized with the perfusion values in Kidney)

Fig. 14 shows the correlation between Kpl and this signal ratio is approximately linear. We also compare Kpl to this ratio map in different organs and two types of tumor showing high amounts of lactate to pyruvate signal in tumor regions(Fig. 15 and Fig. 16)

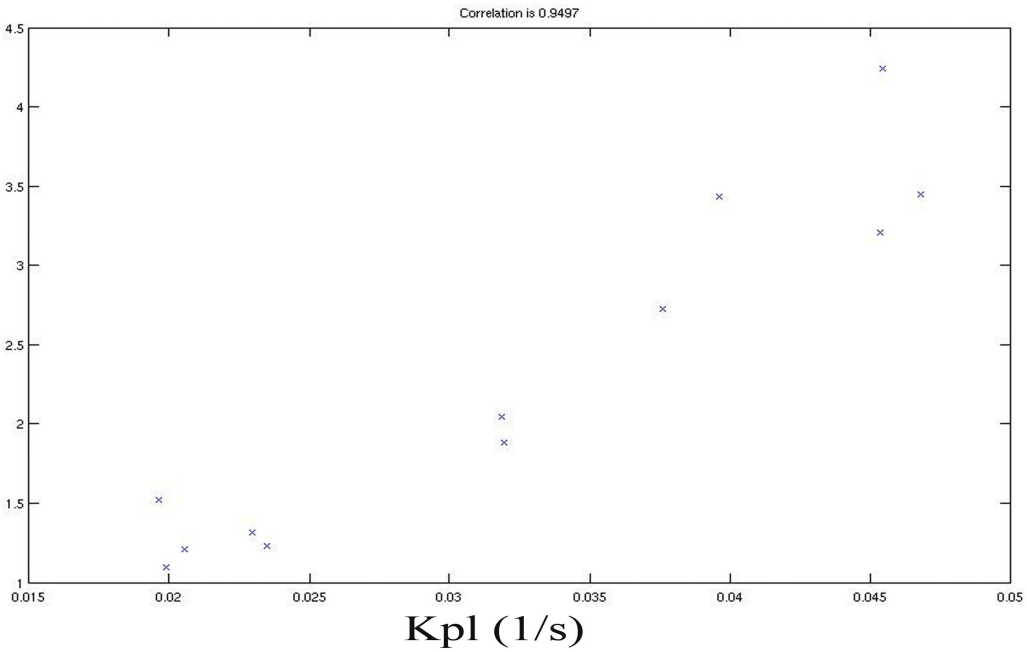

Figure 14. Correlation between Kpl and lactate to Pyruvate signal across kidney, liver, and tumor tissues which had a correlation coefficient of 0.95.

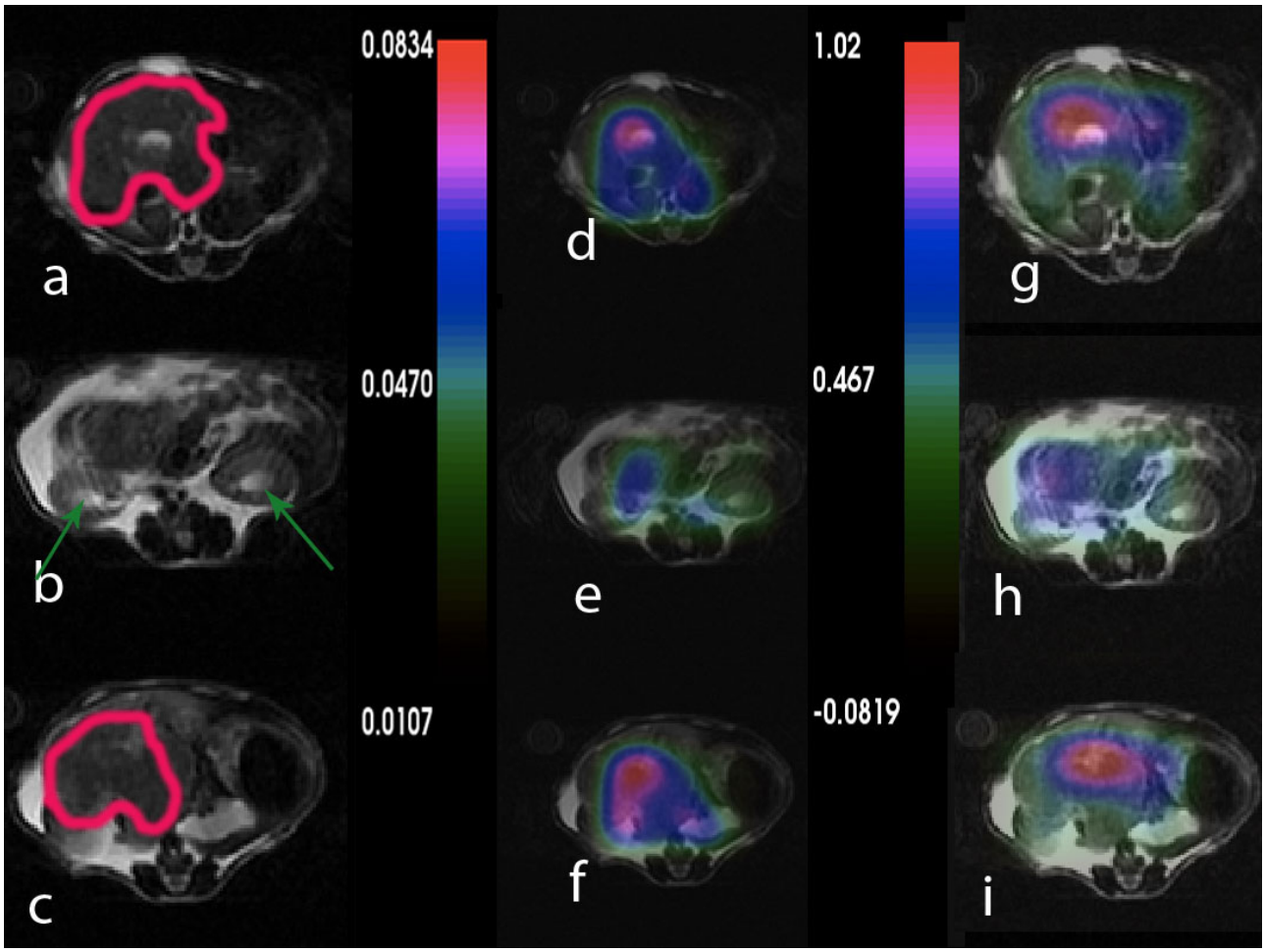

Figure 15. Mapping of the Kpl and lactate to pyruvate signal ratio in different slices of cancerous tissue and healthy tissue. Anatomical images of liver cancer, kidney, and liver including both cancerous and healthy voxels are shown in a), b), and c), respectively. Kidneys(arrows) and cancer tissue(boundaries) are shown Kpl maps in d) liver cancer, e) kidneys, and f) whole liver slices. The lactate to pyruvate signal ratio for the same slices are shown at g),h), and i), respectively.

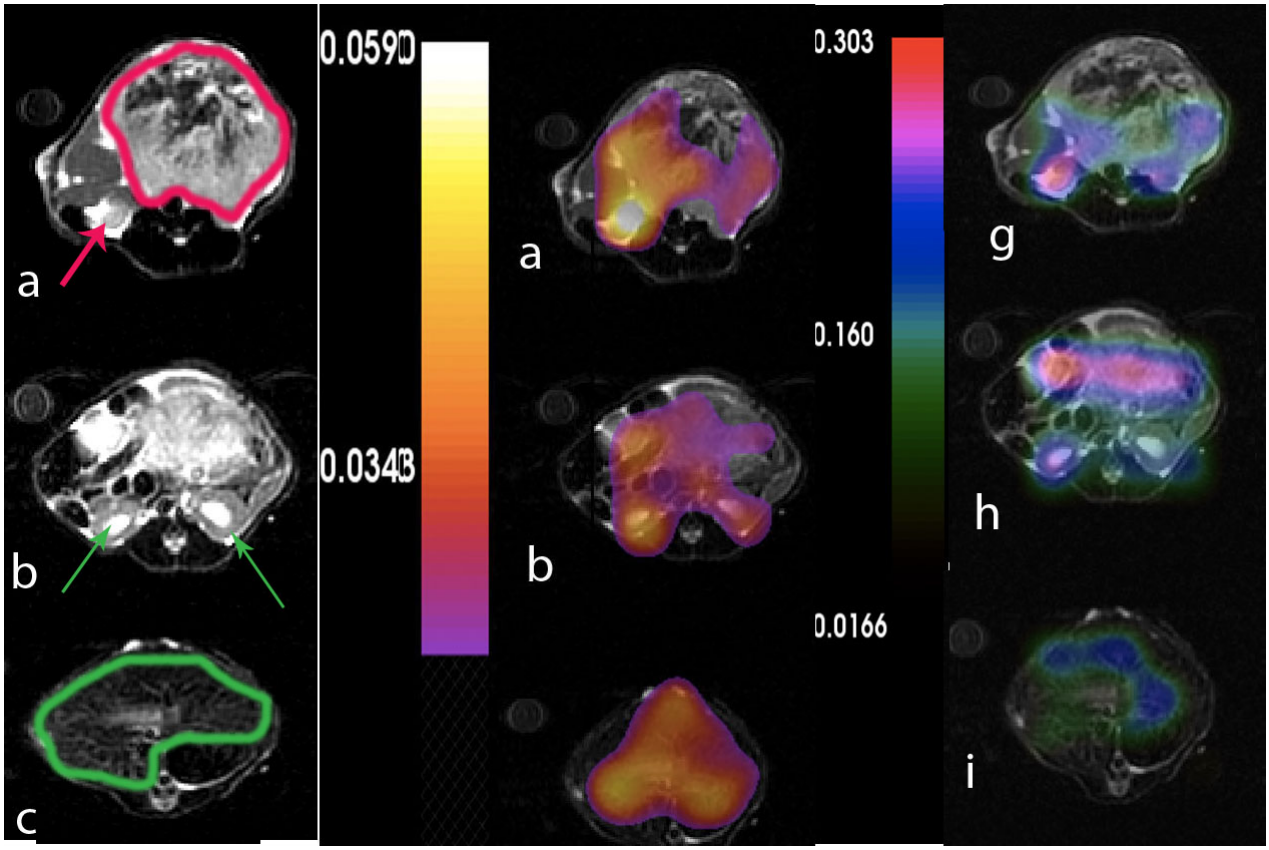

Figure 16. Mapping of the Kpl and lactate to pyruvate signal ratio in different slices of cancerous tissue and healthy tissue Anatomical images of prostate cancer (red boundary), kidney (arrows), and healthy liver (green boundary) slices are shown in a), b), and c), respectively. Kpl maps in d) prostate cancer, e) kidneys, and f) liver slices. The lactate to pyruvate signal ratio for the same slices are shown at g),h), and i), respectively.

An appropriate way in order to validate the model fitting is to repeat fitting of simulated data for different SNRs by adding random noise with various rms. With no noise, the fit with our model was almost perfect. Fig. 17 presents the variation of the model fit Kpl with variation of noise rms showing the model is robust based on the very small amount of change in the fit Kpl with changing noise.

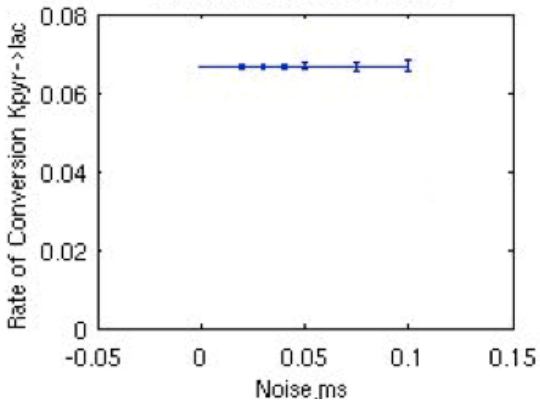

Figure 17. Kpl with changing the noise rms

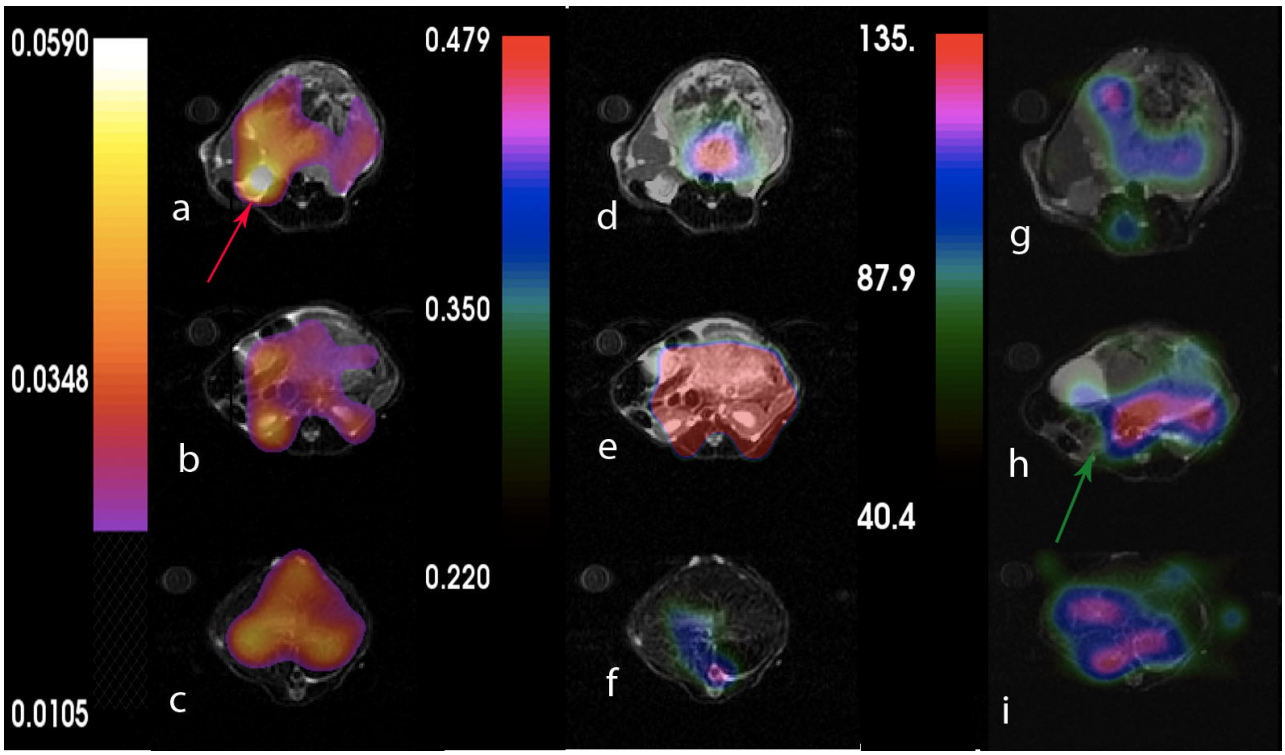

Figure 18. Mapping of Kpl and pyruvate and urea perfusion in different slices of cancerous tissue and healthy tissue, a) Kpl map on the prostate cancer, b)map of the Kpl on kidneys, c) Kpl maps on liver. While the pyruvate perfusion for prostate cancer, kidney, and liver are shown at d),e), and f), respectively. Urea perfusion for prostate cancer, kidney, and liver are shown at g),h), and i), respectively.

We have changed the scale and window level of images in order to acquire better visualization of the metabolites' conversion. Therefore, in Fig.18h) kidneys are marked with arrows. Kpl and perfusion

values of metabolites are mapped at the row image for one subject with prostate cancer in Fig. 18. Showing and visualizing the image and maps simultaneously helped us to follow the parameter changes between voxels. As it is clear and shown with an arrow in Fig.18a) the Kpl values in the cancerous tissues are high. The variation of pyruvate perfusion and urea perfusion can be observed for the healthy and cancerous tissues.

Mapping of the metabolites and other parameters allows us to have better interpretation of the spatial heterogeneity in the tumor as can be observed by varying Kpl values in fig18-a across the tumor. In the prostate tumor slice (Fig 18. a) we can identify a lymph node with metastatic disease in the bottom left of the slice which has a very high Kpl, while low Kpl and low perfusion in parts of primary tumor (more in the center of prostate) are likely necrosis in the animal.

The amount of pyruvate perfusion in fig 18-f in liver is very low. In fig18-g high urea perfusion in the cancerous tissue can be observed and approximately correlates with Kpl.

The same metabolite parameter mapping for one subject with liver cancer is shown in Fig. 19. Showing and visualizing the image and maps simultaneously helped us to follow the parameter changes between the voxels. Obviously, in Fig.18 the Kpl value in the cancerous tissues are high such as in prostate cancer subject. The variation in pyruvate perfusion and urea perfusion can be observed in both healthy and cancerous tissues.

Kpl values in Fig.19a), b), and c) are significantly higher in the liver cancerous tissue(red arrow) with respect to the healthy part of liver(green arrow) and kidney. A small amount of pyruvate perfusion was observed in kidneys in Fig.19f) in comparison to the liver tumor while the urea perfusion as we expected is higher in kidneys(fig.19i).

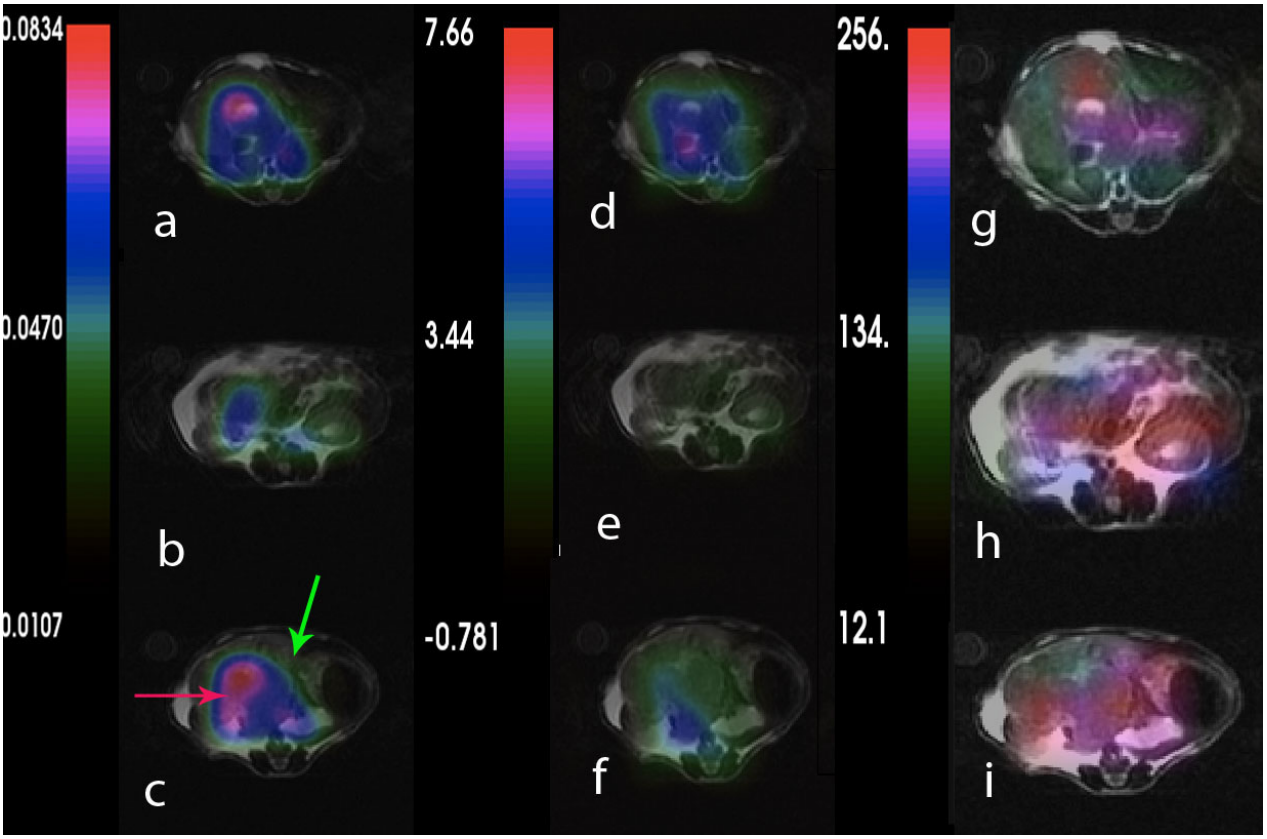

Figure 19. Mapping of the Kpl, pyruvate, and urea perfusion in different slices of cancerous tissue and healthy tissue, a) Kpl map on the liver cancer, b)map of the Kpl on kidneys, c) Kpl maps on liver. While the pyruvate perfusion for prostate cancer, kidney, and liver are shown at d),e), and f), respectively. Urea perfusion for prostate cancer, kidney, and liver are shown at g),h), and i), respectively.

Discussion

The measurement of ρ_1 and metabolite perfusion amount are of practical importance in choosing optimal pulse parameters. In this study, we measured the ρ_1 of tumor hyperpolarized C13 pyruvate and urea. The values reported represent the average ρ_1 values in the tumor. The MRS spectra from which the ρ_1 values were obtained were often contaminated by other organs (partial voluming), and the relaxation times were obtained from all seven animals. (We have observed occasional variability

in the ρ_1 measurements between animals.)

Imperfections of the RF parameters are inevitable in these experiments and they have been a source of many investigations leading to efforts undertaken to eliminate these errors or compensate for them[29]. The fit values for T1s are actually the effective T1 values, and reflect both T1 as well as losses due to flow and pulse sequence imperfection.

Estimation of kinetic model parameters is challenging in vivo due physiologic effects (blood flow, respiratory/cardiac motion) and relatively low SNR in dynamic MRSI. Extracting the T1 of the metabolites is a big step toward finding a standard hallmark of cancerous versus healthy tissues. The range 20-45 (s) looks reasonable[25] for metabolites' T1values which are illustrated in table 1 and table 2.

Measurement of urea perfusion at each organ is proportional to urea concentration in the tissue and can be a marker vascular delivery since urea primarily stays in the vasculature. Liver is a very vascular organ and the opened capillary shape of liver vasculature likely caused high urea perfusion and concentration in liver. The kidneys take up more urea due to their high vasculature and are also responsible for concentrating urine for removal in the urine. In tumor, the tissue request for blood is high but in a more uncontrolled way because of the abnormality of blood vasculature and circulation inside the tumor. The urea perfusion from tumors is more sporadic and random. Urea cannot perfuse well in some parts of tumor particularly in suspected necrotic regions. On the other hand, some parts of tumor have more metabolic activity and, therefore, these parts need more blood and more vessels, and consequently more urea perfusion. The urea perfusion is primarily representing the vasculature delivery in each specific tissue and it stays in the vessels, while the pyruvate perfusion, which is the accumulation of all source and derived metabolites related to the pyruvate including pyruvate, lactate, and alanine, can also be a marker for vascular delivery but also includes tissue uptake. We

hypothesize that when the pyruvate perfusion is higher in some tissues relative to urea perfusion it represents higher amount of uptake of the pyruvate that is flowing into the tissue.

Fixed flip angles were used to acquire all data in this study but can be optimized to improve the model fitting. Future work will include flip angle optimization strategies using simulated data and the presented fitting methods to improve kinetic model parameterization.

Conclusions

In this study we fit metabolite T1 values, Kpa, and Kpl across cancerous and normal tissues from data acquired with a multiband RF excitation dynamic MRSI pulse sequence using two different fitting models. In the first fitting approach we fit the derived longitudinal magnetization using weighted least-squares and for the second fitting approach we used a non-linear least squares algorithm to fit the kinetic model. The conversion constant from pyruvate to lactate and alanine is pretty high in cancerous tissue in comparison to the healthy tissues and lactate signal to pyruvate signal ratio varies commensurate with Kpl, significantly. In the area is suspected to be necrotic tissue, the vasculature network has very low concentration and therefore the amount of urea perfusion is low. The ratio of pyruvate and its products, including lactate and alanine, to urea is significantly higher in cancerous tissues in comparison to healthy tissues which can be marked as a good sign and a marker for cancerous tissue detection.

Our results show that the best prediction and detection of cancerous tissue and its progression in this data set of animals is using NLLS method which is so robust to noise. Analyzing the perfusion among the organs and tissues is also a helpful way for cancerous tissue marking.

References

[1] P. R. Carroll, "Early stage prostate cancer--do we have a problem with over-detection, overtreatment or both?," *J Urol,* vol. 173, pp. 1061-2, Apr 2005.

[2] J. Kurhanewicz, D. B. Vigneron, K. Brindle, E. Y. Chekmenev, A. Comment, C. H. Cunningham, R. J. Deberardinis, G. G. Green, M. O. Leach, S. S. Rajan, R. R. Rizi, B. D. Ross, W. S. Warren, and C. R. Malloy, "Analysis of cancer metabolism by imaging hyperpolarized nuclei: prospects for translation to clinical research," *Neoplasia,* vol. 13, pp. 81-97, Feb 2011.

[3] K. Golman, L. E. Olsson, O. Axelsson, S. Mansson, M. Karlsson, and J. S. Petersson, "Molecular imaging using hyperpolarized 13C," *Br J Radiol,* vol. 76 Spec No 2, pp. S118-27, 2003.

[4] P. J. Kaplan-Lefko, T. M. Chen, M. M. Ittmann, R. J. Barrios, G. E. Ayala, W. J. Huss, L. A. Maddison, B. A. Foster, and N. M. Greenberg, "Pathobiology of autochthonous prostate cancer in a pre-clinical transgenic mouse model," *Prostate,* vol. 55, pp. 219-37, May 15 2003.

[5] J. H. Ardenkjaer-Larsen, B. Fridlund, A. Gram, G. Hansson, L. Hansson, M. H. Lerche, R. Servin, M. Thaning, and K. Golman, "Increase in signal-to-noise ratio of > 10,000 times in liquid-state NMR," *Proc Natl Acad Sci U S A,* vol. 100, pp. 10158-63, Sep 2 2003.

[6] K. Golman and J. S. Petersson, "Metabolic imaging and other applications of hyperpolarized 13C1," *Acad Radiol,* vol. 13, pp. 932-42, Aug 2006.

[7] M. J. Albers, R. Bok, A. P. Chen, C. H. Cunningham, M. L. Zierhut, V. Y. Zhang, S. J. Kohler, J. Tropp, R. E. Hurd, Y. F. Yen, S. J. Nelson, D. B. Vigneron, and J. Kurhanewicz, "Hyperpolarized 13C lactate, pyruvate, and alanine: noninvasive biomarkers for prostate cancer detection and grading," *Cancer Res,* vol. 68, pp. 8607-15, Oct 15 2008.

[8] N. Bahrami, S. H. Rezatofighi, A. M. Adeli, and S. K. Setarehdan, "Boundary delineation for hepatic hemangioma in ultrasound images," *Conf Proc IEEE Eng Med Biol Soc,* vol. 2011, pp. 7989-92, 2011.

[9] J. R. Gingrich, R. J. Barrios, R. A. Morton, B. F. Boyce, F. J. DeMayo, M. J. Finegold, R. Angelopoulou, J. M. Rosen, and N. M. Greenberg, "Metastatic prostate cancer in a transgenic mouse," *Cancer Res,* vol. 56, pp. 4096-102, Sep 15 1996.

[10] N. M. Greenberg, F. DeMayo, M. J. Finegold, D. Medina, W. D. Tilley, J. O. Aspinall, G. R. Cunha, A. A. Donjacour, R. J. Matusik, and J. M. Rosen, "Prostate cancer in a transgenic mouse," *Proc Natl Acad Sci U S A,* vol. 92, pp. 3439-43, Apr 11 1995.

[11] P. Bernatowicz, J. Kowalewski, and S. Szymanski, "Nuclear-spin relaxation in nonrigid molecules: discrete multisite local dynamics combined with

anisotropic molecular reorientation," *J Chem Phys,* vol. 124, p. 024108, Jan 14 2006.
[12] R. J. Gillies, P. A. Schornack, T. W. Secomb, and N. Raghunand, "Causes and effects of heterogeneous perfusion in tumors," *Neoplasia,* vol. 1, pp. 197-207, Aug 1999.
[13] A. P. Chen, M. J. Albers, C. H. Cunningham, S. J. Kohler, Y. F. Yen, R. E. Hurd, J. Tropp, R. Bok, J. M. Pauly, S. J. Nelson, J. Kurhanewicz, and D. B. Vigneron, "Hyperpolarized C-13 spectroscopic imaging of the TRAMP mouse at 3T-initial experience," *Magn Reson Med,* vol. 58, pp. 1099-106, Dec 2007.
[14] P. Vaupel, F. Kallinowski, S. Runkel, K. Schlenger, and H. P. Fortmeyer, "Blood flow and oxygen consumption rates of human gynecological tumors xenografted into rnu/rnu-rats," *Strahlenther Onkol,* vol. 165, p. 502, Jul 1989.
[15] I. Park, P. E. Larson, M. L. Zierhut, S. Hu, R. Bok, T. Ozawa, J. Kurhanewicz, D. B. Vigneron, S. R. Vandenberg, C. D. James, and S. J. Nelson, "Hyperpolarized 13C magnetic resonance metabolic imaging: application to brain tumors," *Neuro Oncol,* vol. 12, pp. 133-44, Feb 2010.
[16] P. E. Larson, S. Hu, M. Lustig, A. B. Kerr, S. J. Nelson, J. Kurhanewicz, J. M. Pauly, and D. B. Vigneron, "Fast dynamic 3D MR spectroscopic imaging with compressed sensing and multiband excitation pulses for hyperpolarized 13C studies," *Magn Reson Med,* vol. 65, pp. 610-9, Mar 2011.
[17] T. H. Witney, M. I. Kettunen, D. E. Hu, F. A. Gallagher, S. E. Bohndiek, R. Napolitano, and K. M. Brindle, "Detecting treatment response in a model of human breast adenocarcinoma using hyperpolarised [1-13C]pyruvate and [1,4-13C2]fumarate," *Br J Cancer,* vol. 103, pp. 1400-6, Oct 26 2010.
[18] S. E. Day, M. I. Kettunen, F. A. Gallagher, D. E. Hu, M. Lerche, J. Wolber, K. Golman, J. H. Ardenkjaer-Larsen, and K. M. Brindle, "Detecting tumor response to treatment using hyperpolarized 13C magnetic resonance imaging and spectroscopy," *Nat Med,* vol. 13, pp. 1382-7, Nov 2007.
[19] S. Hu, A. Balakrishnan, R. A. Bok, B. Anderton, P. E. Larson, S. J. Nelson, J. Kurhanewicz, D. B. Vigneron, and A. Goga, "13C-pyruvate imaging reveals alterations in glycolysis that precede c-Myc-induced tumor formation and regression," *Cell Metab,* vol. 14, pp. 131-42, Jul 6 2011.
[20] C. G. Koay, L. C. Chang, J. D. Carew, C. Pierpaoli, and P. J. Basser, "A unifying theoretical and algorithmic framework for least squares methods of estimation in diffusion tensor imaging," *J Magn Reson,* vol. 182, pp. 115-25, Sep 2006.
[21] A. Mishra, Y. Lu, A. S. Choe, A. Aldroubi, J. C. Gore, A. W. Anderson, and Z. Ding, "An image-processing toolset for diffusion tensor tractography," *Magn Reson Imaging,* vol. 25, pp. 365-76, Apr 2007.
[22] A. W. Anderson, "Theoretical analysis of the effects of noise on diffusion tensor imaging," *Magn Reson Med,* vol. 46, pp. 1174-88, Dec 2001.
[23] L. C. Chang, D. K. Jones, and C. Pierpaoli, "RESTORE: robust estimation of tensors by outlier rejection," *Magn Reson Med,* vol. 53, pp. 1088-95, May 2005.

[24] M. Puckeridge, G. Pages, and P. W. Kuchel, "Simultaneous estimation of T(1) and the flip angle in hyperpolarized NMR experiments using acquisition at non-regular time intervals," *J Magn Reson,* vol. 222, pp. 68-73, Sep 2012.
[25] C. von Morze, P. E. Larson, S. Hu, H. A. Yoshihara, R. A. Bok, A. Goga, J. H. Ardenkjaer-Larsen, and D. B. Vigneron, "Investigating tumor perfusion and metabolism using multiple hyperpolarized (13)C compounds: HP001, pyruvate and urea," *Magn Reson Imaging,* vol. 30, pp. 305-11, Apr 2012.
[26] A. P. Chen, J. Kurhanewicz, R. Bok, D. Xu, D. Joun, V. Zhang, S. J. Nelson, R. E. Hurd, and D. B. Vigneron, "Feasibility of using hyperpolarized [1-13C]lactate as a substrate for in vivo metabolic 13C MRSI studies," *Magn Reson Imaging,* vol. 26, pp. 721-6, Jul 2008.
[27] C. Boesch, "Molecular aspects of magnetic resonance imaging and spectroscopy," *Mol Aspects Med,* vol. 20, pp. 185-318, Aug-Oct 1999.
[28] S. Josan, Y. F. Yen, R. Hurd, A. Pfefferbaum, D. Spielman, and D. Mayer, "Application of double spin echo spiral chemical shift imaging to rapid metabolic mapping of hyperpolarized [1-(1)(3)C]-pyruvate," *J Magn Reson,* vol. 209, pp. 332-6, Apr 2011.
[29] L. Bosman, P. K. Madhu, S. Vega, and E. Vinogradov, "Improvement of homonuclear dipolar decoupling sequences in solid-state nuclear magnetic resonance utilising radiofrequency imperfections," *J Magn Reson,* vol. 169, pp. 39-48, Jul 2004.

Publishing Agreement

It is the policy of the University to encourage the distribution of all theses, dissertations, and manuscripts copies of all UCSF theses, dissertations, and manuscripts will be routed to the library via the Graduate Division. The library will make all theses, dissertations, and manuscripts accessible to the public and will preserve these to the best of their ability, in perpetuity.

Please sign the following statement:

I hereby grant permission to the Graduate Division of the University of California, San Francisco to release copies of my thesis, dissertation, or manuscript to the Campus Library to provide access and preservation, in whole or in part, in perpetuity.

N. Bath

Author Signature

08/02/2013

Date